Mineralogical control on critical companion metal distribution: Expanded workflow, with examples from the Sullivan Pb-Zn-Ag deposit

Luke Ootes[1, a], Audrey C. Graham[1], Keani Whitmore[1, 2], Dylan Goudie[3], Stephen J. Piercey[4], Shaun Barker[5], Sarah Milne[5], and Chris McFarlane[6]

[1] British Columbia Geological Survey, Ministry of Mining and Critical Minerals, Victoria, BC, V8W 9N3
[2] School of Earth and Ocean Sciences, University of Victoria, Victoria, BC, V8W 3P6
[3] Core Research Equipment and Instrument Training (CREAIT) Network, Memorial University of Newfoundland, St. John's, NL, A1C 5S7
[4] Department of Earth Sciences, Memorial University of Newfoundland, St. John's, NL, A1B 1N3
[5] Mineral Deposit Research Unit, University of British Columbia, Vancouver, BC, V8W 3P6
[6] Department of Earth Sciences, University of New Brunswick, Fredericton, NB, E3B 5A3
[a] corresponding author: Luke.Ootes@gov.bc.ca

Recommended citation: Ootes, L., Graham, A.C., Whitmore, K., Goudie, D., Piercey, S.J., Barker, S., Milne, S., and McFarlane, C., 2026. Mineralogical control on critical companion metal distribution: Expanded workflow, with examples from the Sullivan Pb-Zn-Ag deposit. In: Geological Fieldwork 2025, British Columbia Ministry of Mining and Critical Minerals, British Columbia Geological Survey Paper 2026-01, pp. 45-52.

Abstract

Relative to primary ore metals (e.g., Cu, Zn) critical companion metals (e.g., In, Sn, PGEs, Te) generally occur in low concentrations and, although typically not exploration targets, they can represent significant by- or co-product opportunities during mining. Understanding the distribution and coupling or decoupling of these companion metals with primary ore metals will help further understand their distribution in deposits and their potential economic viability. We use samples from the past-producing Sullivan Pb-Zn-Ag mine to illustrate an expanded workflow for critical mineral projects at the British Columbia Geological Survey. Geochemical analyses, thin section petrography, and quantitative mineralogy by scanning electron microscope-mineral liberation analysis (SEM-MLA) are successful in identifying major and trace minerals. However, some minerals contain minor elements in solid solution that SEM-MLA is unable to identify. For these elements the workflow required expansion and micro x-ray fluorescence (μXRF) analysis was added as an element mapping tool. Whole rock geochemical analyses from some samples of Sullivan mineralization yielded >100 ppm In, but neither the SEM-MLA nor μXRF work resolved the mineralogical host. Thus, we also employed elemental mapping by laser ablation-inductively coupled-plasma mass spectrometry (LA-ICP-MS). This mapping revealed that even though the minor phase cassiterite (SnO_2) contains the highest In concentrations, In is predominantly hosted in solid solution in sphalerite. Cassiterite is uncommon in the samples investigated and Sn is predominantly in boulangerite ($Pb_5Sb_4S_{11}$). These results indicate that Sn and In are coupled in cassiterite but decoupled and in solid solution in boulangerite (Sn) and sphalerite (In), an observation significant for the exploration and production of these metals. The expanded workflow and tool combination provide quantitative insights into metal coupling and decoupling in mineralization and can be applied in cases where mineralogical control on elemental distribution is elusive.

Keywords: Critical companion metals, LA-ICP-MS, SEM-MLA, μXRF, Sullivan

1. Introduction

Relative to primary ore metals (e.g., Cu, Zn) critical companion metals (e.g., Sn, PGEs, Te) generally occur in low concentrations and, although typically not exploration targets, they can represent significant by- or co-product opportunities during mining (e.g., Holley et al., 2025). For example, sedimentary exhalative (SEDEX) and related deposits in predominantly siliciclastic successions contain primary commodities Pb, Zn, and Ag and can contain recoverable concentrations of companion metals (e.g., Ge, Sn, In). These companion metals can occur either as discrete mineralogical phases (e.g., cassiterite, SnO_2) or as solid solution substitutions in the crystal lattice of other minerals, such as trace metals in sphalerite (e.g., Bonnet et al., 2016), or in sulphosalts (e.g., Moëlo et al., 2008). Understanding the distribution and coupling or decoupling of these companion metals with primary ore metals will help further understand their distribution in deposits and their potential economic viability. To resolve this in British Columbia mineral deposits, the application of modern analytical techniques is required to quantify mineralogical control on critical companion metals (e.g., Wei et al., 2026).

Using quantitative geochemical analysis, Graham et al. (2025) demonstrated abundances of Sn and In at the past-producing Sullivan Pb-Zn-Ag deposit. However, the mineralogical relationship of these companion metals to the primary ore metals remains unresolved. In this study, we use the same samples as Graham et al. (2025) to identify the host

minerals at Sullivan and to detail a modified version of the project workflow for critical minerals (Piercey et al., 2025), which combines Zeiss Axioscan petrographic images with scanning electron microscope-mineral liberation analysis (SEM-MLA) expanded to include micro x-ray fluorescence analysis (μXRF). This combined approach determined the host mineralogical phase of most metals (e.g., Sb, As) but was only partially successful for some metals (e.g., Sn) and failed for others (e.g., In). To further constrain the mineralogical control on elemental distribution we also conducted elemental mapping by laser ablation-inductively coupled plasma-mass spectrometry (LA-ICP-MS).

2. Methods and workflow

The ten samples used in this study come from the past-producing Sullivan mine (Fig. 1) and represent a range of mineralization styles from the deposit including massive sulphide from the 'Main ore band' and 'Bedded ore bands'. These samples were previously collected and stored in the British Columbia Geological Survey (BCGS) rock archive (Rukhlov et al., 2023). Geochemical results from these rocks are presented in Graham et al. (2025) and Graham and Ootes (2025). Sample offcuts were prepared as polished thin sections.

The BCGS has adopted the mineral systems approach to its critical minerals projects (e.g., Hickin et al., 2024). Analytical work prioritizes: 1) producing mines; 2) past-producing mines; 3) advanced exploration projects; and 4) showings and prospects. Geochemical analysis is the first step in quantifying metal contents of samples (Fig. 2; e.g., Graham et al., 2025; Piercey et al., 2025). Samples that contain critical companion metals are followed up with petrographic analysis and mineralogical quantification using scanning electron microscope-mineral liberation analysis (SEM-MLA). This study also conducted micro x-ray fluorescence (μXRF) analysis to determine elemental distributions (Fig. 2). For elemental distribution (e.g., Sn, In) that could not be resolved by these methods, laser ablation-inductively coupled plasma-mass spectrometry (LA-ICP-MS) analysis was employed. This geochemical and micro-analytical workflow provides quantification of mineralogical control on critical companion metals (Figs. 2-5; Tables 1, 2).

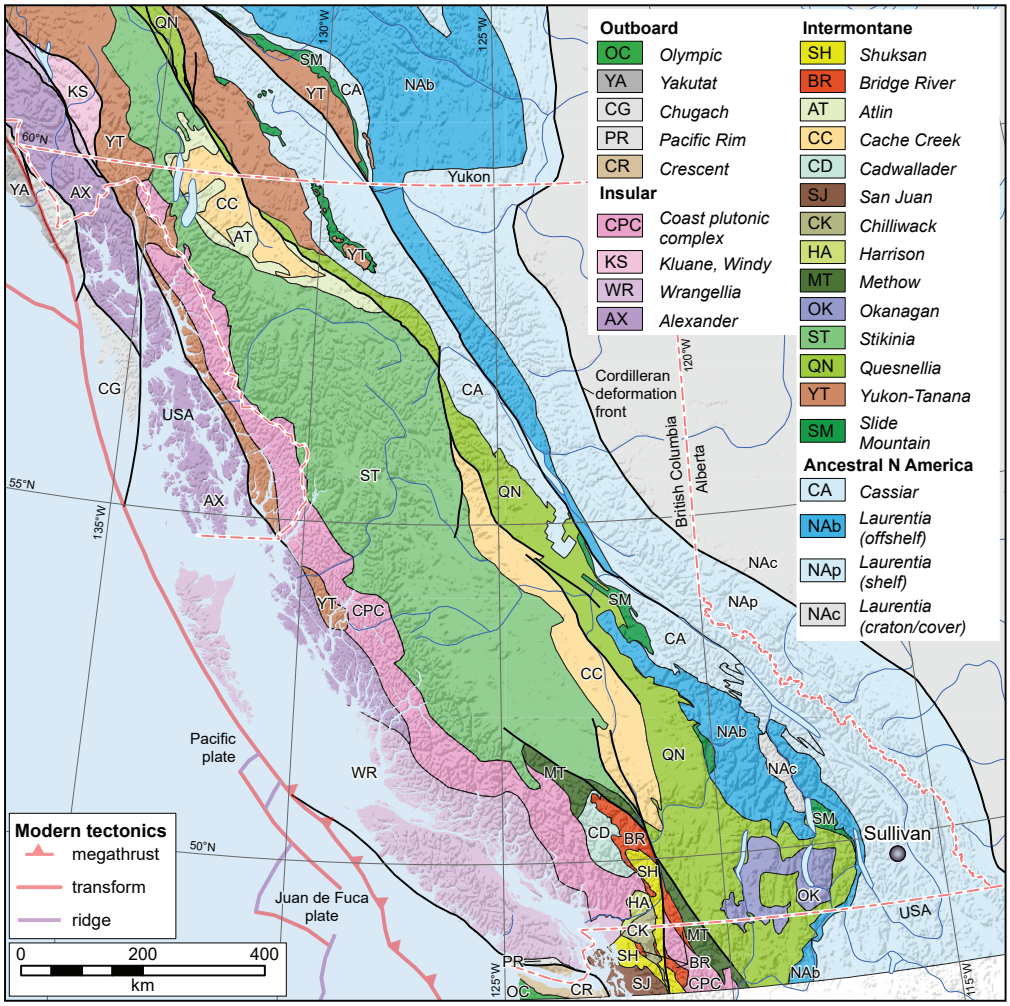

Fig. 1. Location of the Sullivan deposit. Terranes after Colpron (2020).

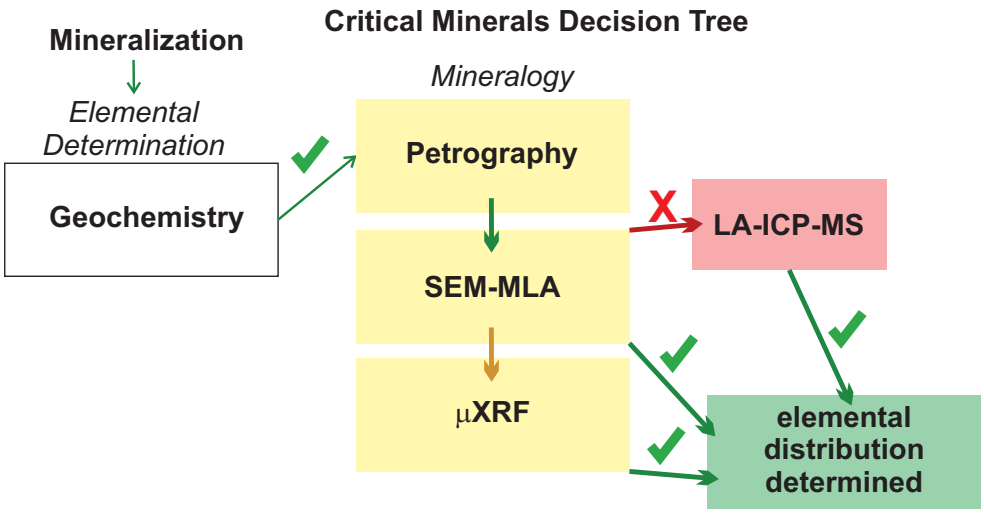

Fig. 2. Decision tree and workflow for critical companion metals projects at the British Columbia Geological Survey, expanded after Piercey et al. (2025). Green check marks and arrows indicate positive determination of mineral host to metals. Orange arrow indicates that only a subset of samples are investigated with μXRF. Red X and arrow indicate that LA-ICP-MS analysis is required for determination.

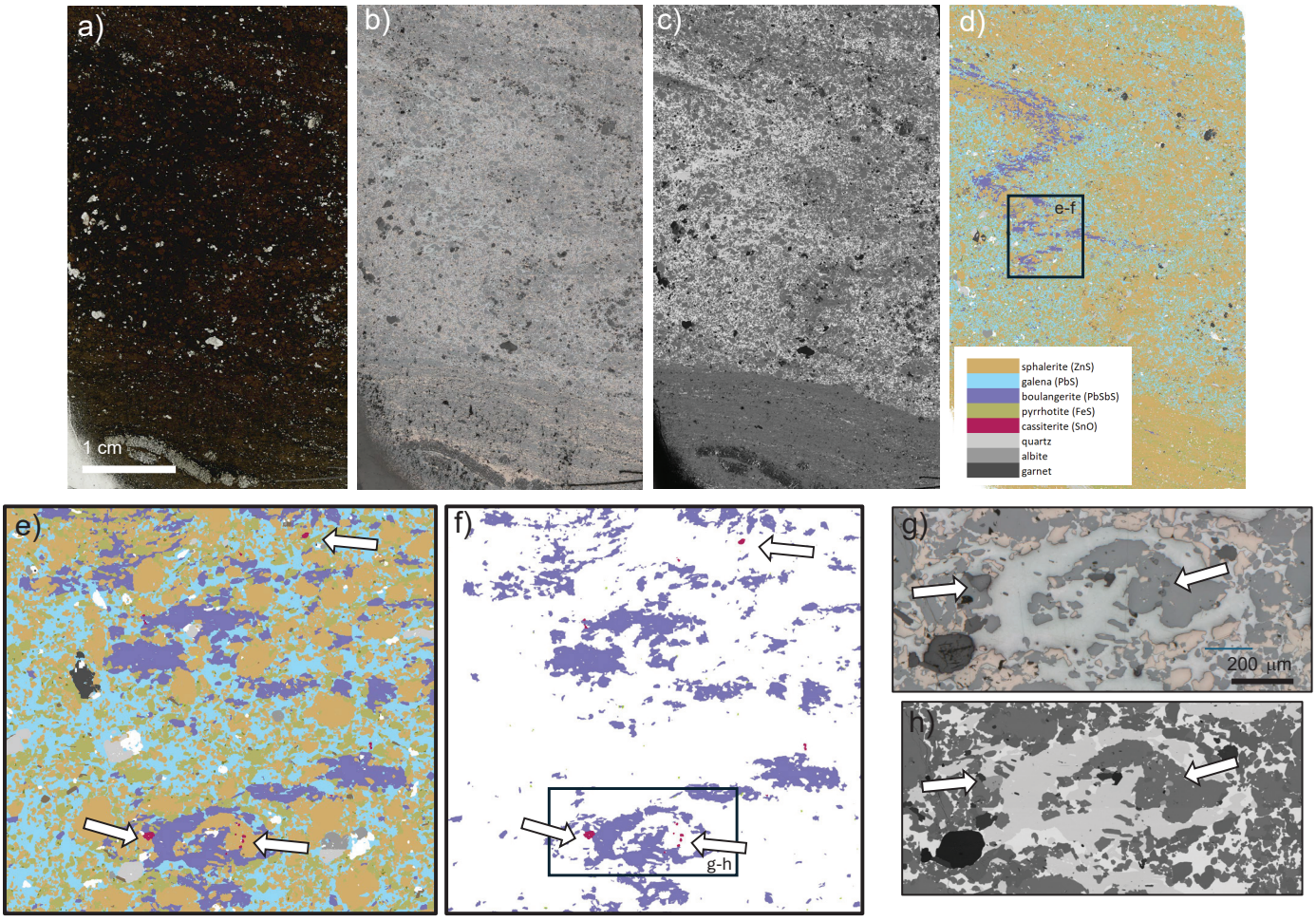

Fig. 3. Thin section images of a Sullivan Main band sample. **a)** Photomicrograph, plane polarized light. **b)** Photomicrograph, reflected light. **c)** Backscattered electron (BSE) image. **d)** False colour MLA image; legend applies to images d-f. **e-f)** Examples using false colour MLA, including resampling colours, to find trace minerals in samples using cassiterite (SnO_2; arrows) as an example. **g)** Reflected light and **h)** BSE images that highlight the difficulty of finding cassiterite without the use of MLA.

2.1. Petrography

Polished thin sections were prepared and automated petrographic images were created using Zeiss Axioscan Geo7 at the University of British Columbia, Mineral Deposits Research Unit. These images include plane, polarized, circular polarized, and reflected light photomicrographs that are hosted online and have real-time pan and zoom functionality (Figs. 3a, b). This system allows the petrographer the ability to conduct thin-section-scale to micron-scale mineralogical and textural evaluation of samples and allows heads-up comparison with other datasets.

2.2. Scanning electron microscope-mineral liberation analysis

To assist in the mineralogical and elemental assessment, automated mineralogical mapping using SEM-MLA was conducted at CREAIT Microanalysis Facility (MAF), Memorial University of Newfoundland. Polished thin sections were mapped using a scanning electron microscope with derived backscatter electron (BSE) images and quantitative mineral abundance maps by mineral liberation analysis. The SEM work used a FEI MLA 650 field emission gun SEM equipped with two Brucker silicon drift EDS detectors. Operating conditions included 25 kV accelerating voltage for BSE images. Operating conditions for MLA included a 25 kV accelerating voltage, 10 nA current, and a 5.85 electron beam spot size. Thin sections were measured in GXMAP (grain-based x-ray mapping) mode where x-ray analyses were triggered for a BSE range of 40 to 255. Each x-ray measurement was acquired for 12 ms on a 1.5 by 1.5 mm frame with a resolution of 500 pixels per frame and an imaging scan speed of 16 µsec. Data reduction was performed on MLA Data View (FEI) software version 3.1.4.683.

The SEM-MLA provides full thin-section data as BSE images and false colour mineralogical maps (Figs. 3c, d). In-house Python™ coding enables rapid colour changes to MLA images, highlighting different mineral phases and allowing comparison to photomicrographs and BSE images (Figs. 3e-h). Each false-colour MLA image is accompanied by a quantitative

Table 1. Selected results of SEM-MLA quantitative mineralogy from a Main band sample, Sullivan deposit (see Figure 3).

Mineral	Wt.%	Area%	Area (micron)	Particle Count	Grain Count
Total	100.00	100.00	732005342.97	1698	267375
Sphalerite	41.29	48.71	356544422.34	1033	51383
Galena	35.64	22.73	166385090.57	770	121430
Pyrrhotite	19.15	19.58	143328920.14	649	59969
Quartz	1.55	2.79	20454776.04	422	5709
Boulangerite	0.57	2.68	19596283.07	345	4047
Albite	0.45	0.82	5987058.75	369	1399
Fe-Ca Rhodocrosite	0.13	0.64	4652136.87	404	3103
Chlorite	0.36	0.57	4154413.57	391	3999
Biotite	0.33	0.51	3711215.97	397	3837
Mn-Fe-Ca Garnet	0.09	0.42	3065875.40	227	1032
Pyrite	0.25	0.24	1738439.48	411	6021
Muscovite	0.06	0.10	758617.92	268	1384
Mn Siderite	0.02	0.10	720595.37	272	903
Fe Mg Al silicate	0.01	0.03	214244.55	201	450
Apatite	0.01	0.02	159740.81	193	567
Tetrahedrite	0.02	0.02	152710.37	286	739
Chalcopyrite	0.02	0.02	132941.72	223	422
Ilmenite	0.01	0.01	64393.56	150	273
Cassiterite	0.01	0.01	63504.46	76	113

Table 2. Selected elemental concentrations of sulphide minerals from LA-ICP-MS mapping (see Figure 5).

Mineral	S^{34}	±2s	Fe^{56}	±2s	Zn^{66}	±2s	Pb^{208}	±2s	Sn^{118}	±2s	Sb^{121}	±2s	Ag^{107}	±2s	Cd^{111}	±2s	Bi^{209}	±2s	In^{115}	±2s
	ppm		ppm		ppm		ppm		ppm		ppm		ppm		ppm		ppm		ppm	
Pyrrhotite	524572.9	31452.0	467533.2	15885.9	1539.4	791.7	36504.2	47308.0	3.1	4.0	63.3	63.5	4.6	1.7	11.4	7.9	2.5	2.6	0.2	0.3
Pyrrhotite	507374.0	20327.4	439852.3	37386.1	6778.0	7866.3	11884.9	10424.8	2.3	2.0	387.6	142.9	13.1	10.2	79.0	87.5	0.5	0.4	4.7	5.7
Pyrrhotite	494821.7	19443.5	432786.5	36634.6	9234.7	6979.6	62382.6	49823.5	8.0	6.5	409.7	264.7	69.5	54.9	91.6	91.2	4.1	3.2	11.7	10.6
Sphalerite	387786.7	8980.3	44968.2	1205.3	564239.6	9156.7	172.8	27.6	0.1	0.0	11.3	5.7	3.3	0.4	1739.6	26.3	0.0	0.0	149.4	5.3
Sphalerite	394380.3	8468.6	47534.5	955.2	554846.5	8004.2	383.4	66.9	0.1	0.0	13.0	4.2	3.7	0.5	1812.2	63.2	0.0	0.0	144.8	3.7
Sphalerite	386068.3	3497.1	48790.0	961.7	561909.0	3152.1	190.7	18.8	0.4	0.1	18.7	3.8	6.7	2.1	2007.5	61.2	0.0	0.0	148.1	3.5
Cassiterite	32258.0	20948.0	9176.8	6742.1	28451.9	30026.4	9043.7	3948.0	852277.5	126511.0	1853.2	811.6	2.8	3.0	97.9	92.1	0.8	0.6	2731.5	390.2
Boulangerite	216566.2	4804.8	56.2	14.3	306.4	191.4	618679.6	8086.2	121.3	3.6	164088.2	4672.0	55.0	23.7	21.7	41.0	49.5	0.9	0.5	0.0
Boulangerite	220102.8	2944.5	367.7	568.5	419.7	256.3	615125.6	5485.7	139.0	4.7	163966.4	4996.3	24.2	4.2	1.4	0.5	49.8	1.4	0.6	0.0
Boulangerite	221223.1	5516.2	50.0	8.6	127.3	23.8	613742.6	7113.5	135.0	3.5	164576.0	3069.5	25.4	2.0	0.8	0.1	53.1	1.0	0.6	0.0
Galena	109358.7	6675.0	50.6	17.3	112.9	25.9	889886.0	6760.4	37.6	2.0	764.7	57.4	698.8	61.7	8.4	0.9	19.5	0.5	0.2	0.0
Galena	122687.3	5615.9	228.8	90.7	254.7	99.1	876202.4	5641.9	43.6	2.4	822.9	38.8	732.4	34.5	9.7	2.6	20.8	0.4	0.2	0.1
Galena	130036.5	5893.6	218.4	192.5	187.9	91.6	868667.4	5776.0	35.4	1.1	1096.3	629.0	705.3	36.6	7.8	0.8	28.8	0.5	0.2	0.0

±2s refers to the internal standard error

mineralogical table that specifies the mineral species in the sample and the spatial distribution and number of crystals in the sample (Table 1).

2.3. μXRF

A Bruker TornadoPlus μXRF instrument fitted with two 60 mm^2 detectors, housed in the Mineral Deposit Research Unit, University of British Columbia, was used for analysis. An Rh x-ray tube, excited to 50 kV and 600 nA current generated x-rays, which are focused through a polycapillary x-ray optic on the sample. The x-ray spot generated has a diameter of ~19 mm. Data were collected with a spatial resolution of 50 mm (generating images with a pixel resolution of 50 by 50 mm), with a counting time of 10 ms per pixel, typically generating several thousand x-ray counts per pixel. Sampling occurs as a sequential line scan, whereby the 19 mm spot moves along the sample as the instrument stage travels from left to right, the stage then steps back to its starting point, travels 100 mm down, and then travels left to right again. Data were processed in Bruker ESPRIT® software. In the software, a colour stretch is applied to count data so that higher counts appear as brighter colours producing intensity maps. Finally, a fundamental parameter (FP) method in Bruker ESPRIT® software was applied to each map to quantify results, which accounts for peak overlaps and background corrections. Because no standards were analyzed with unknown samples, the results should be treated as semi-quantitative, with significant uncertainties on any individual pixel. However, the FP method has the advantage that it helps the viewer to determine likely 'true' variations in element intensities in a sample by removing variations in count rates caused by sample geometry and colour stretches, which are applied across very low count rate elements. Colours that occur outside the edge of the sample represent artefacts introduced by the background substrate of the samples and should be taken as being inaccurate.

2.4. Laser ablation-inductively coupled plasma-mass spectrometry

To support the SEM-MLA and μXRF results, the metal distribution was mapped by LA-ICP-MS analysis in the Department of Earth Sciences, University of New Brunswick (Table 2). Two samples with high In were targeted, and in each thin section four sub-areas were chosen based on textural and mineralogical diversity (Fig. 5). Trace-element raster maps were acquired using an Applied Spectra Inc. ASI RESOlution 193 nm laser ablation system connected to an Agilent 8900 QQQ-ICP-MS. A Norris Scientific 'fast-funnel' and Quadlock™ device were used to achieve fast washout and eliminate spectra skew. Rectangular areas of interest were ablated using a series of raster lines space at 25 mm and using a laser beam diameter of 26 mm, a pulse rate set by the Quadlock system (18-19 Hz), and a stage scan speed of 60 mm/s. The ICP-MS was set to collect a suite of 24 elements (^{24}Mg, ^{27}Al, ^{29}Si, ^{31}P, ^{34}S, ^{39}K,^{44}Ca, ^{47}Ti, ^{55}Mn, ^{56}Fe, ^{63}Cu, ^{66}Zn, ^{71}Ga, ^{73}Ge, ^{75}As, ^{107}Ag, ^{111}Cd, ^{115}In, ^{118}Sn, ^{121}Sb, ^{125}Te, ^{208}Pb, and ^{209}Bi) with a total quadrupole sweep

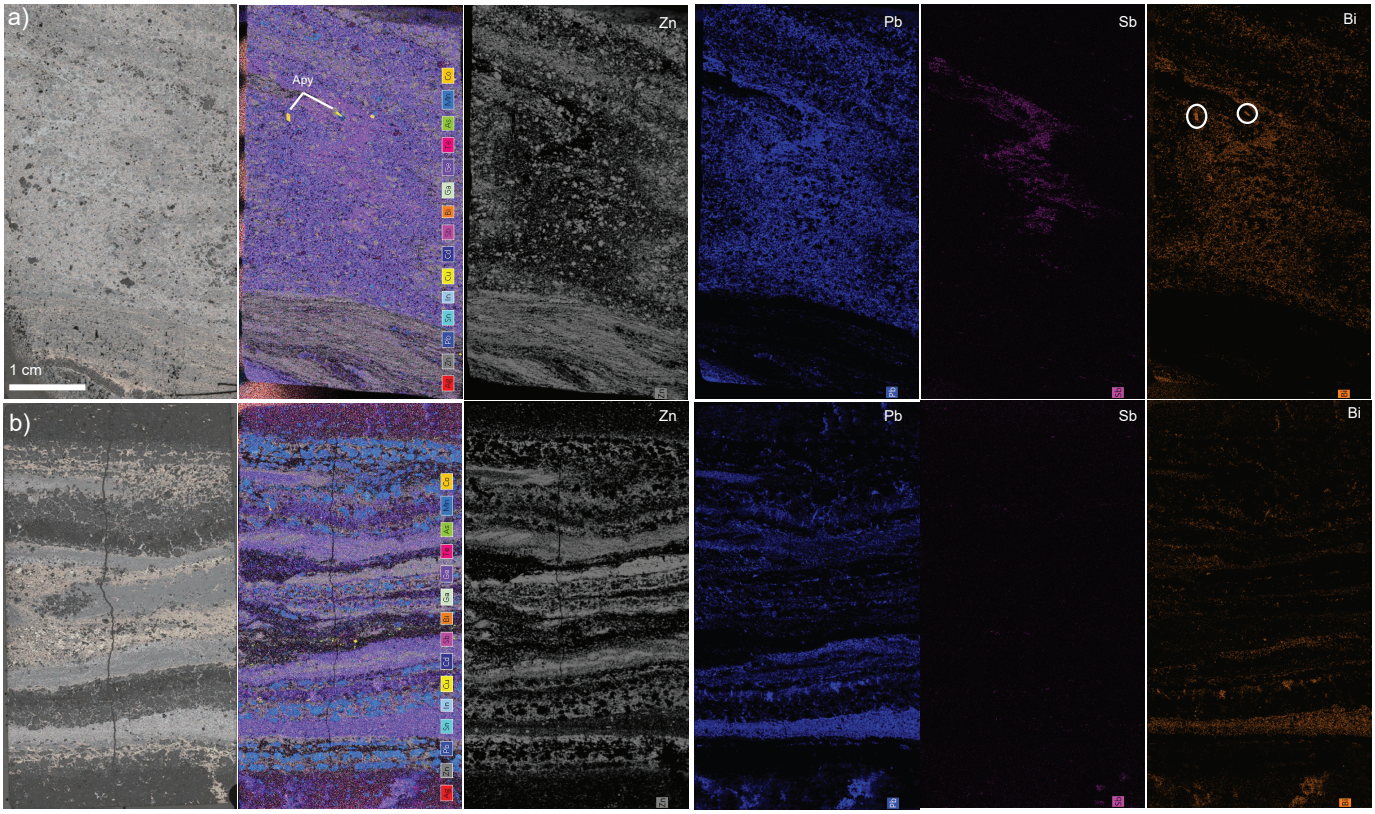

Fig. 4. Results of µXRF scans. Samples from **a)** Sullivan Main band. **b)** Sullivan C band. Left to right: photomicrograph (reflected light); full colour µXRF; results for Pb, Zn, Sb, and Bi. Because µXRF was conducted on thin section cutoffs, the photomicrograph and µXRF images do not exactly match.

time <0.25 s. The instrumentation was tuned on NIST610 glass to obtain oxide production (^{248}ThO/^{232}Th) <0.2%, doubly charged production (22 M/^{44}Ca) <0.2%, and ^{238}U/^{232}Th of 1.02. Standards USGS BCR2-G and MASS-1 were also measured throughout the run to act as primary and secondary standards.

Trace-element maps were produced offline using Iolite4 and the 3D Trace-element Data Reduction Scheme that includes a normalization to 100% calculation approach obviating the need for internal standardization. The 3D Trace-element DRS also includes a criteria function to parse mineral phases based on major-element compositions (e.g., Pb for galena; Zn for sphalerite; Fe for pyrite and pyrrhotite; Sb for boulangerite; Si for silicates; Sn for cassiterite). This allows full quantification of trace-element maps (e.g., Fig. 5) on the basis of observed mineralogy. Mean concentrations are derived from circular regions of interest selected on several examples of each mineral in the laser map.

3. Discussion

Petrographic and SEM-MLA quantitative mineralogy (Fig. 3; Table 1) demonstrates the ability to identify various mineralogical phases. For example, a boulangerite ($Pb_5Sb_4S_{11}$) band (Fig. 3d) is segregated from galena (PbS) indicating that Sb is localized and concentrated in Sullivan ore, rather than being uniformly distributed throughout, consistent with mine-scale metal distribution (Freeze, 1966). Rare and tiny (<100 mm) cassiterite crystals (SnO_2) only occur locally in this sample (Table 1), and these were only found through interrogation of the false-colour MLA image (Figs. 3e-f); these crystals would be difficult to find and identify using reflected light petrography or BSE images alone (Figs. 3g, h). However, unlike Sb-in-boulangerite and Sn-in-cassiterite, some minerals contain minor elements in solid solution that SEM-MLA was unable to identify.

The application of µXRF to thin section offcuts provides maps of elemental distribution (Fig. 4). Zinc and Pb do not form solid-solution minerals together, and their decoupling as sphalerite and galena-boulangerite is clear on the µXRF images. The µXRF results agree with the MLA observations that Sb is segregated (Fig. 4a). Bismuth minerals (e.g., bismuthinite; Bi_2S_3) are uncommon in the Sullivan samples. However, µXRF shows that Bi is distributed within galena-boulangerite and trace arsenopyrite crystals (Fig. 4). The same is true for Sn (not shown). This indicates solid solution within boulangerite and galena (Pb and Sb) and decoupling from sphalerite (Zn; Fig. 4).

The Sullivan Main band sample (Figs. 3, 4a, 5) contains >100 ppm In (Graham et al., 2025; Graham and Ootes, 2025), but neither the SEM-MLA nor µXRF could resolve the In distribution, and LA-ICP-MS analysis was employed. Those results, along with all other resultant data maps, were

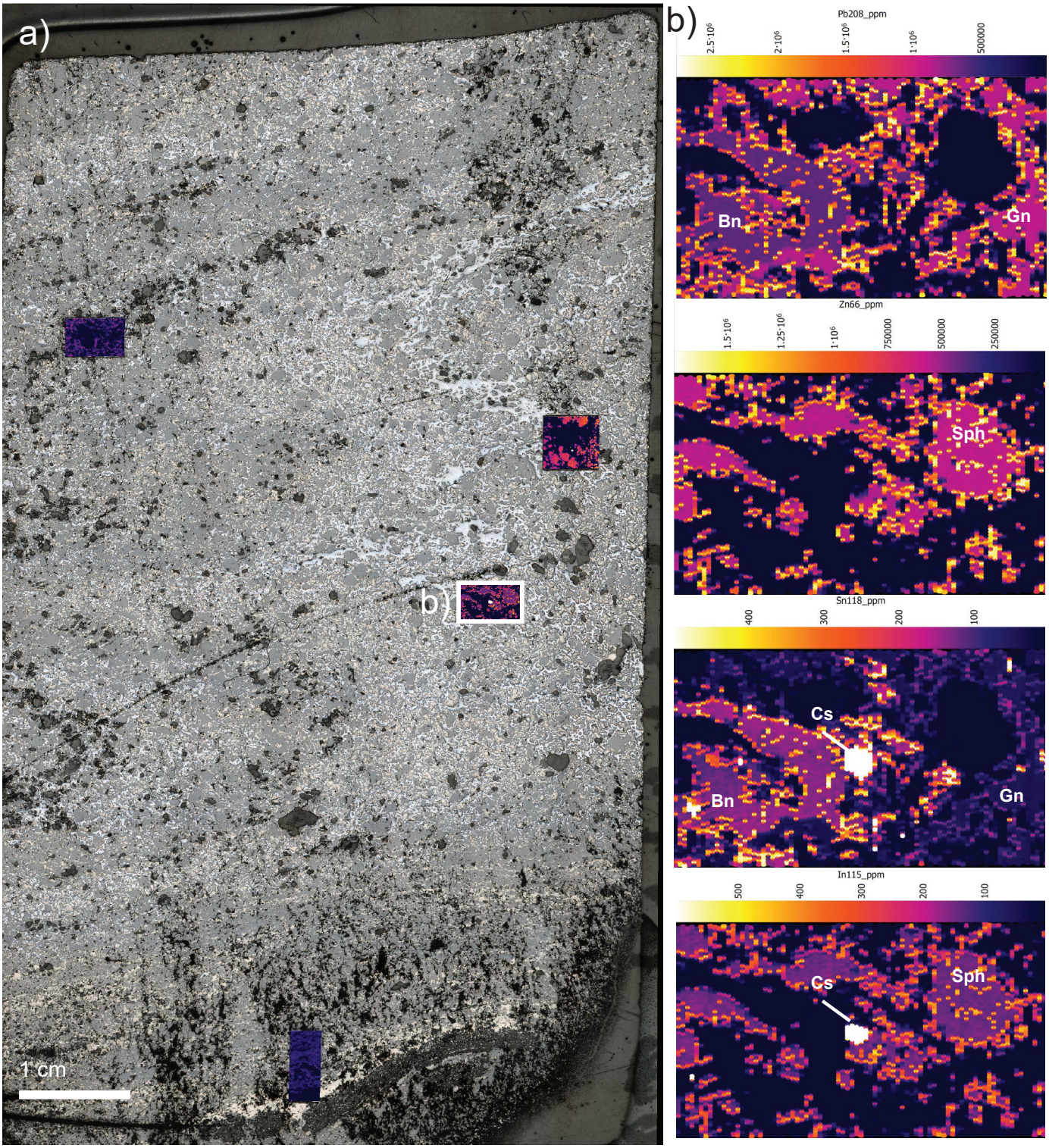

Fig. 5. a) Thin section photomicrograph of the Sullivan Main band (reflected light). The four coloured boxes are the locations of LA-ICP-MS elemental maps, all showing the distribution ^{115}In. **b)** Examples of elemental distribution of one of the mapped areas. From top to bottom are elemental distributions on ^{208}Pb, ^{66}Zn, ^{118}Sn, and ^{115}In. The circular white mineral in the Sn and In maps is cassiterite (see Figure 3). Colour ramps are in parts per million (ppm).

georeferenced (Fig. 5); for simplicity here we use the reflected light photomicrograph of Sullivan Main band sample as a base. Each coloured box on Figure 5a are the In distribution maps from LA-ICP-MS. Elemental comparison (Fig. 5b) highlights the distribution of Pb, Zn, Sn, and In in the mapped area. An isolated cassiterite crystal contains the highest concentration of In in the sample (~2700 ppm; Table 2), indicating In is preferentially hosted in cassiterite (Fig. 5b). Additional In is hosted in sphalerite (~150 ppm; Table 2). In both cases, the In is in solid solution within these minerals.

As outlined below, these data offer a tentative interpretation that envisages coupling of Sn-In-in-cassiterite and decoupling of Sn-in-boulangerite and In-in-sphalerite, which has significant exploration and production implications. Because cassiterite is an oxide, the massive sulphide zone of the Sullivan main band would have been oxygen deficient. Thus, once oxygen in the system was exhausted, the Sn could no longer form as cassiterite and needed an alternative mineral host. The LA-ICP-MS maps and data show secondary abundance of Sn-in-boulangerite, but not in galena or sphalerite (Table 2; Figs. 3, 5). The maps and data also show secondary abundance of In-in-sphalerite, but not in boulangerite or galena. It may have been that excess Sn moved into solid solution in boulangerite and that the remaining In, which also required a mineralogical home, was accommodated by sphalerite (Fig. 5b). Acknowledging that this is a preliminary interpretation and limited LA-ICP-MS mapping, if elemental coupling and decoupling occurs at a deposit-scale, understanding and quantifying this distribution and mineralogical control would be paramount in the exploration for and production of these metals.

4. Conclusion

The expanded workflow for critical minerals projects at the BCGS allows the identification and quantification of the mineralogical control and distribution of critical companion metals in mineral systems. The combination of petrography, SEM-MLA, and μXRF is sufficient to identify mineralogical phases and elemental distribution. In some cases, the resolving power of LA-ICP-MS is required to identify elemental phases and their mineralogical control. The benefit of SEM-MLA is thin section-scale analysis that can be combined with whole rock geochemical results, whereas the μXRF provides fine-scale, high-spatial resolution results that quantify the distribution of otherwise unfindable trace metals.

Acknowledgment

We thank Brian McNulty for comments to an early draft that improved this contribution.

References cited

Bonnet, J., Mosser-Ruck, R., Caumon, M-C., Rouer, O., Andre-Myer, A-S., Cauzid, J., and Peiffert, C., 2016. Trace element distribution (Cu, Ga, Ge, Cd, and Fe) in sphalerite from the Tennessee MVT deposits, USA, by combined EMPA, LA-ICP-MS, Raman spectroscopy, and crystallography. The Canadian Mineralogist, 54, 1261-1284. <https://doi.org/10.3749/canmin.1500104>

Colpron, M., 2020. Yukon terranes-A digital atlas of terranes for the northern Cordillera. Yukon Geological Survey. <https://data.geology.gov.yk.ca/Compilation/2#InfoTab>

Freeze, A.C., 1966. On the origin of the Sullivan orebody, Kimberley, BC. British Columbia Geological Survey, Property File 680182, 194 p.

Graham, A.C., and Ootes, L., 2025. Geochemical analyses of SEDEX deposits in eastern British Columbia. British Columbia Ministry of Mining and Critical Minerals, British Columbia Geological Survey GeoFile 2025-13, 9 p.

Graham, A.C., Wearmouth, C.D., Northcote, B., and Ootes, L., 2025. A preliminary assessment of critical companion elements in SEDEX deposits of eastern British Columbia: Examples from the historic Sullivan mine and the Cirque project. In: Geological Fieldwork 2024, British Columbia Ministry of Mining and Critical Minerals, British Columbia Geological Survey Paper 2025-01, pp. 141-152.

Holley, E.A., Hadden, K.M., Hammerling, D., Eggert, R., Spiller, D.E., and Nelson, P.P., 2025. By-product recovery from US metal mines could reduce import reliance for critical minerals, Science, 389, 1325-1331. <https://doi.org/10.1126/science.adw8997>

Hickin, A.S., Ootes, L., Orovan, E.A., Brzozowski, M.J., Northcote, B.K., Rukhlov, A.S., and Bain, W.M., 2024. Critical minerals and mineral systems in British Columbia. In: Geological Fieldwork 2023, British Columbia Ministry of Energy, Mines and Low Carbon Innovation, British Columbia Geological Survey Paper 2024-01, pp. 13-51.

Moëlo, Y., Makovicky, E., Mozgova, N.N., Jambor, J.L., Cook, N., Pring, A., Paar, W., Nickel, E.H., Graeser, S., Karup-Møller, S., Balic-Žunic, T., Mumme, W.G., Vurro, F., Topa, D., Bindi, L., Bente, K., and Shimizu, M., 2008. Sulfosalt systematics: a review. Report of the sulfosalt sub-committee of the IMA Commission on Ore Mineralogy. European Journal of Mineralogy, 20, 7-46. <https://doi.org/10.1127/0935-1221/2008/0020-1778>

Piercey, S.J., Pietruszka, D., and Goudie, D., 2025. Critical metals in volcanogenic massive sulphide (VMS) deposits in British Columbia: A progress report. In: Geological Fieldwork 2024, British Columbia Ministry of Mining and Critical Minerals, British Columbia Geological Survey Paper 2025-01, pp. 189-201.

Rukhlov, A.S., Coats, B., Van der Vlugt, J., Beaupre-Olsen, I.J., and Zaborniak, K., 2023. British Columbia Geological Survey sample archive: An emerging resource for public geoscience. In: Geological Fieldwork 2022, British Columbia Ministry of Energy, Mines and Low Carbon Innovation, British Columbia Geological Survey Paper 2023-1, pp. 85-90.

Wei, C., Pietruszka, D.K., Piercey, S.J., Aylward, W., Kommescher, S., Scanlan, E., and Layton-Matthews, D., 2026. Critical metal distributions in volcanogenic massive sulphide (VMS) deposits in British Columbia: A progress report. In: Geological Fieldwork 2025, British Columbia Ministry of Mining and Critical Minerals, British Columbia Geological Survey Paper 2026-01, pp. 53-67.